Enhancing magneto-optic effects in two-dimensional magnets by thin-film interference

Hendriks, Freddie; Guimarães, Marcos H. D.

Published in:
AIP Advances

DOI:
10.1063/5.0040262

Publication date:
2021

Enhancing magneto-optic effects in two-dimensional magnets by thin-film interference

Cite as: AIP Advances 11, 035132 (2021); doi: 10.1063/5.0040262
Submitted: 22 January 2021 • Accepted: 3 March 2021 •
Published Online: 18 March 2021

F. Hendriks[a] and M. H. D. Guimarães[a]

AFFILIATIONS

Zernike Institute for Advanced Materials, University of Groningen, 9747 AG Groningen, The Netherlands

[a]Authors to whom correspondence should be addressed: f.hendriks@rug.nl and m.h.guimaraes@rug.nl

ABSTRACT

The magneto-optic Kerr effect is a powerful tool for measuring magnetism in thin films at microscopic scales, as was recently demonstrated by the major role it played in the discovery of two-dimensional (2D) ferromagnetism in monolayer CrI_3 and $Cr_2Ge_2Te_6$. These 2D magnets are often stacked with other 2D materials in van der Waals heterostructures on a SiO_2/Si substrate, giving rise to thin-film interference. This can strongly affect magneto-optical measurements but is often not taken into account in experiments. Here, we show that thin-film interference can be used to engineer the magneto-optical signals of 2D magnetic materials and optimize them for a given experiment or setup. Using the transfer matrix method, we analyze the magneto-optical signals from realistic systems composed of van der Waals heterostructures on SiO_2/Si substrates, using CrI_3 as a prototypical 2D magnet, and hexagonal boron nitride to encapsulate this air-sensitive layer. We observe a strong modulation of the Kerr rotation and ellipticity, reaching several tens to hundreds of milliradians, as a function of the illumination wavelength, and the thickness of SiO_2 and layers composing the van der Waals heterostructure. Similar results are obtained in heterostructures composed by other 2D magnets, such as $CrCl_3$, $CrBr_3$, and $Cr_2Ge_2Te_6$. Designing samples for the optimal trade-off between magnitude of the magneto-optical signals and intensity of the reflected light should result in a higher sensitivity and shorter measurement times. Therefore, we expect that careful sample engineering, taking into account thin-film interference effects, will further the knowledge of magnetization in low-dimensional structures.

Magneto-optical effects, such as the Kerr and Faraday effect, are key to unveiling the magnetic structure and spin behavior of low-dimensional systems.[1–5] In these effects, a change in the reflected or transmitted light intensity and polarization is (often linearly) related to the change in magnetization of the illuminated area. When used in combination with microscopy techniques, magneto-optical signals can be used to image the magnetization of systems at the sub-micrometer scale,[6–8] and when combined with ultrafast lasers, they give access to the magnetization dynamics at femtosecond timescales.[9–13] The magneto-optic Kerr effect (MOKE) was instrumental for the discovery of two-dimensional (2D) ferromagnetism in monolayer CrI_3 and $Cr_2Ge_2Te_6$.[14,15] Due to its non-destructive nature and easy implementation, MOKE and related magneto-optic effects, such as reflected magnetic circular dichroism, are one of the standard tools for the magnetic characterization of 2D van der Waals magnets.[5,14–17] For those measurements, 2D magnets are often stacked with other van der Waals materials on a substrate, such as hexagonal boron nitride (hBN) on SiO_2/Si substrates. These layered systems can display strong thin-film interference effects, which, in turn, affect their magneto-optical response. At the start of the 2D materials revolution, it was discovered that exploiting these interference effects allowed for optical identification of graphene flakes,[18–20] providing a way for easily identifying graphene mono- or few-layers. Later, the same techniques were used for identifying thin layers of other van der Waals materials, such as transition metal dichalcogenides.[21–24] In addition, the effects of thin-film interference on magneto-optical signals, and how to use these effects to enhance them, have been studied extensively in the context of metallic thin-films,[25–30] oriented molecular films,[31] ellipsometry,[32–34] and many other fields. However, thin-film interference

effects are often not taken fully into account for the magneto-optical experiments on van der Waals magnets.[35,36] This could lead to a sub-optimal signal-to-noise ratio, resulting in a lower sensitivity and/or longer measurement times. Therefore, it becomes more difficult and more time-consuming to measure small changes in magnetization of 2D magnets caused by, for example, chiral spin textures in a homogeneously magnetized lattice and to measure under low-light conditions to avoid sample degradation. While some works do take into account the effect of the oxide substrate, hBN, or a polymer layer on the magneto-optical signals,[37–41] a comprehensive study of thin-film interference effects for the magneto-optics in realistic samples is still lacking.

Here, we show that not only the substrate but also other materials in a van der Waals stack can greatly affect the MOKE signals and that these signals can be significantly enhanced by carefully choosing the illumination wavelength and through heterostructure engineering (Fig. 1), as is well known from other studies on thin-film interference enhancements of MOKE signals from, e.g., metallic thin films. Using a transfer matrix approach for thin-film interference, we demonstrate that the MOKE signals can reach values of tens to hundreds of milliradians at sizable reflected light intensities. In particular, we explore this effect on three systems based on the 2D van der Waals magnet CrI_3 on a SiO_2/Si substrate: monolayer CrI_3, bulk CrI_3, and monolayer CrI_3 encapsulated in hBN (we also consider other 2D magnets, see the supplementary material). Our results show that the often disregarded hBN encapsulation used to protect the air-sensitive 2D magnet films can strongly affect the magnitude of the MOKE signals such that subtler magnetic textures in 2D magnets can be measured.

We model the thin layered systems as a series of stacked parallel homogeneous layers, where the first and the last layer (being air and Si) are semi-infinite. An example of this geometry is illustrated in Fig. 1(a), where a single 2D magnetic layer of thickness t_{2DM} is on top of a SiO_2/Si substrate with oxide thickness t_{ox}. The interfaces are assumed to be smooth such that there are only specular reflections. Furthermore, we assume that the illumination intensity is low enough such that the optical properties of the materials can be described by a linear dielectric permittivity tensor ε and magnetic permeability tensor μ. The intensity and polarization of the light that reflects off this stratified linear system are calculated using the transfer matrix method. We use a method similar to the one in Ref. 26, which is explained in full detail in the supplementary material.

The transfer matrix relates the components of the electric ($\vec{E}$) and magnetic ($\vec{H}$) field parallel to the layers, called $\vec{E}_\parallel$ and $\vec{H}_\parallel$, respectively, at one interface of a medium to the other one. To construct a transfer matrix, we start by describing plane waves in a single layer. We begin from the Maxwell equations in isotropic homogeneous media and consider plane waves with a frequency ω and wave vector $\vec{k}$ of the form $\vec{E} = \vec{E}_0 \exp(i(\vec{k}\cdot\vec{r} - \omega t))$, where t is the time and $\vec{r}$ is the position in space. We can then derive the following wave equation:

$$\boldsymbol{\varepsilon}^{-1}\left(\vec{k}\times\left(\boldsymbol{\mu}^{-1}\left(\vec{k}\times\vec{E}_0\right)\right)\right) = -\omega^2\vec{E}_0. \tag{1}$$

Solving the above-mentioned equation yields four values for the z-component of $\vec{k}$, $k_{z,i}$, and four corresponding polarization eigenmodes, $\vec{E}_{0,i}$, where i labels the polarization mode. These solutions describe two plane waves traveling in the $+z$ direction and two in the $-z$ direction. The transfer matrix is the diagonal matrix $\mathrm{diag}(\exp(ik_{z,i}t_{\mathrm{layer}}))$, which propagates the eigenmodes with wave vector components $k_{z,i}$ from one interface to the other one over a distance t_{layer}, after it is transformed from the basis of the eigenmode amplitudes to the basis of the amplitudes of the $\vec{E}_\parallel$ and $\vec{H}_\parallel$ components. The transfer matrix of the whole system is simply the product of the transfer matrices of the individual layers since $\vec{E}_\parallel$ and $\vec{H}_\parallel$ are continuous across the interfaces. This matrix is used to calculate the amplitudes of the eigenmodes of the reflected and transmitted light and from this the reflected intensity and polarization.

We apply the above-mentioned method to the system illustrated in Fig. 1(a), where the 2D ferromagnet is monolayer CrI_3 with a thickness of $t_{2DM} = 0.7$ nm. The dielectric tensor of ferromagnetic monolayer CrI_3 is taken from the study by Wu *et al.*, [39] where it is calculated from first-principles methods taking excitonic effects into account. The dielectric constants of Si and thermally grown SiO_2 are experimental values taken from the study by Herzinger *et al.*[42] The magnetic permeability of all materials is approximated by the scalar vacuum permeability μ_0. Using these parameters, we calculate the Kerr angle θ_K, Kerr ellipticity ε_K, and reflected intensity of linearly polarized light hitting the sample at normal incidence and polar

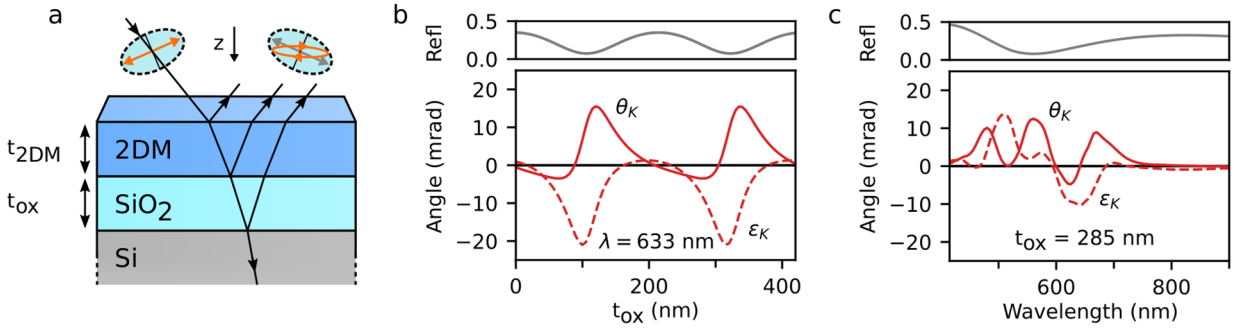

FIG. 1. (a) Typical 2D ferromagnet sample displaying the MOKE in the presence of thin-film interference. (b) and (c) The calculated Kerr rotation and ellipticity depend heavily on the oxide thickness and wavelength. The maximum signal occurs when the reflectivity is close to its minimum.

configuration. The results are shown in Figs. 1(b) and 1(c) as a function of t_{ox} and wavelength, respectively.

Figure 1(b) shows a clear periodic behavior of the MOKE signals as a function of t_{ox}, with a period of 216 nm, corresponding to half a wavelength in SiO_2. It also shows that the Kerr angle and ellipticity attain their maximum values when the reflected intensity is close to a minimum, and vice versa. In Fig. 1(c), the largest MOKE signals are found in the wavelength range from 400 to 750 nm, where the wavelength dependence of θ_K and ε_K is caused primarily by the wavelength dependence of the dielectric tensor of CrI_3. Again, θ_K and ε_K attain their maximum values when the reflectivity is close to a minimum. These results show that the oxide thickness and the wavelength of the light have a strong impact on the sign and magnitude of the MOKE signals. By optimizing t_{ox} or the wavelength, the signals can already change by as much as 20 mrad in this example, while still having a sizable reflectivity of more than 6%.

In order to get a complete picture of the impact of each parameter on the signals, we explore the full parameter space, varying both the wavelength and oxide thickness for a CrI_3 monolayer on a SiO_2/Si substrate (Fig. 2). Besides the reflectivity, θ_K, and ε_K, we also calculate the contrast for the CrI_3 layer. This can be used to locate the target flake, usually a few μm in size and therefore hard to find on a large substrate, using a microscope or using a reflectivity scan in a laser based experiment. The contrast is defined as $C = (I - I_0)/I_0$, where I and I_0 are the reflected intensity of the system with and without CrI_3, respectively. The reflectivity in Fig. 2 shows a clear fan pattern. The periodicity in t_{ox} in our simulated reflectivity corresponds to half a wavelength in the SiO_2, which strongly suggests that this fan pattern is caused by the interference of the light reflected from the top and bottom interface of the SiO_2, similar to graphene-based systems.[20] The same pattern appears for C, θ_K, and ε_K, indicating that the interference in the SiO_2 layer also has a large effect on the contrast and MOKE signals. Additional features at 420, 500, and 680 nm can also be seen, and they originate from the wavelength dependence of the dielectric tensor of CrI_3 (see the supplementary material). By tuning both the wavelength and oxide thickness, θ_K and ε_K can be tuned over a range of several tens of milliradians while keeping the reflectivity above 5%. Furthermore, when the Kerr rotation and ellipticity are maximized, the contrast is large as well, making it easier to locate the CrI_3 using, e.g., a simple reflectivity scan.

The above-mentioned results can be compared to the experimental results from the study by Huang *et al.*[14] In their experimental work, using a laser with a wavelength of 633 nm and t_{ox} = 285 nm, they obtained $\theta_K = 5 \pm 2$ mrad. Our theoretical result of 3.5 mrad is within the experimental error margin. Our results are also in agreement with the absence of an experimental signal at a wavelength of 780 nm for this system. We find that the MOKE signals at these wavelengths are reduced by about a factor of 10 and could easily be obscured by the experimental noise. Figure 1 also indicates that the combination of an oxide thickness of 285 nm and a laser wavelength of 633 nm does not result in the largest Kerr rotation. Using an oxide thickness of 335 nm instead would increase θ_K by more than a factor of 4, or if the wavelength is changed to 560 nm, the Kerr rotation can increase by a factor of about 3.

The 2DM thickness can also strongly affect the MOKE signals. Figure 3 shows the dependence of the magneto-optical signals as a function of both wavelength and 2DM thickness, using the dielectric tensor of ferromagnetic bulk CrI_3 taken from the study by Wu *et al.*[39] While the theoretical values of ε_{CrI_3} used in our calculations differ slightly from the available experimental values,[14,43] our main findings are not altered if we consider the experimental values. We, therefore, opt for using the theoretical values since they span a larger wavelength range. For comparison, we provide calculations using the experimental values in the supplementary material.

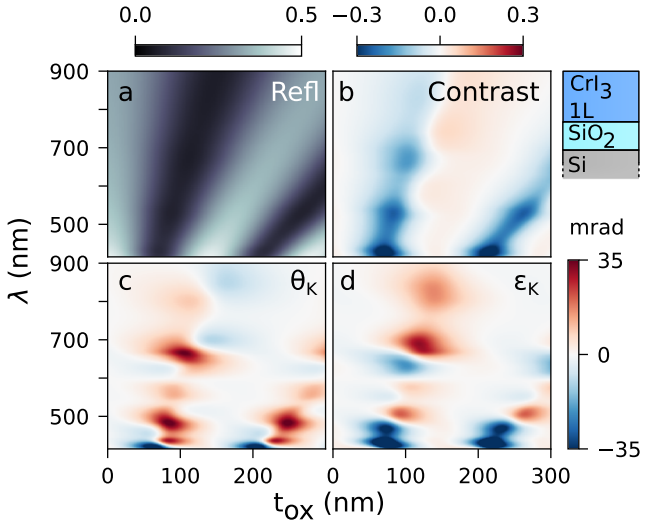

FIG. 2. Simulation results for a CrI_3(1L)-SiO_2-Si stack. (a) Reflectivity, (b) contrast, (c) Kerr rotation, and (d) ellipticity are shown as a function of illumination wavelength and oxide thickness. Where the color scale is saturated, the values exceed the bounds of the scale.

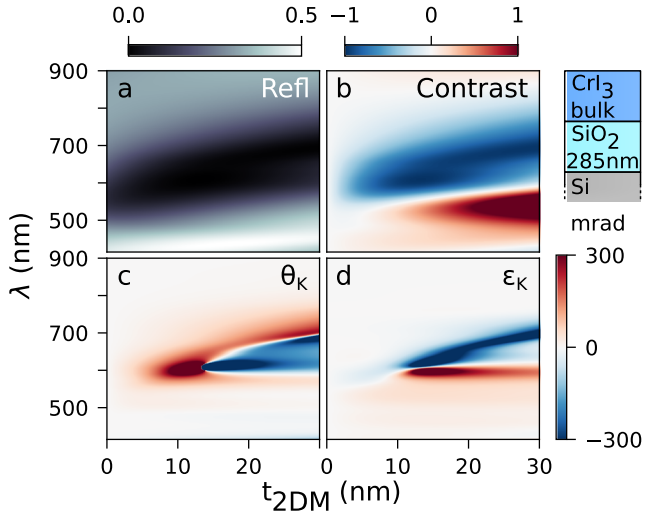

FIG. 3. Simulation results for a CrI_3(bulk)-SiO_2(285 nm)-Si stack. (a) Reflectivity, (b) contrast, (c) Kerr rotation, and (d) ellipticity are shown as a function of wavelength and CrI_3 thickness. Where the color scale is saturated, the values exceed the bounds of the scale.

Interestingly, θ_K and ε_K have a non-monotonic behavior, showing a strong peak and dip around a wavelength of 600 nm and a CrI_3 thickness of 14 nm. The extreme values of θ_K and ε_K approach $\pm\pi/2$ and $\pm\pi/4$, respectively. The reflectivity at these points is around 0.2% for the maximum Kerr rotation and 0.4% for the maximum Kerr ellipticity. These extreme MOKE signals can, therefore, be very hard to detect. However, θ_K and ε_K can still be changed over a range of a few hundred milliradians when tuning the wavelength and CrI_3 thickness, while keeping the reflectivity above 5% and having a good contrast.

Due to the air sensitivity of many 2DMs, they are often encapsulated in hBN.[35,36] The presence of the hBN layers also leads to thin-film interference effects and thus can be used to engineer the magneto-optical signals as well.[40] To explore the impact of hBN encapsulation, we study the MOKE signals in monolayer CrI_3 encapsulated by a top and bottom hBN flake with the same thickness t_{hBN}. The refractive index of hBN needed for the simulation is calculated using the single oscillator model, $n(\lambda)^2 = 1 + A\lambda^2/(\lambda^2 - \lambda_0^2)$, where $\lambda_0 = 164.4$ nm and $A = 3.263$ are determined experimentally by Lee *et al.*[44] The simulation results for an oxide layer of 285 nm are shown in Fig. 4. We have also investigated the effect of the hBN thickness on the signal-to-noise ratio (see the supplementary material). A striking result is that an hBN thickness of about 10 nm, a typical thickness for hBN flakes used for encapsulation in experimental studies, can already lead to dramatic changes in the reflectivity, contrast, and Kerr signals. Therefore, one should take into account the system as a whole when engineering their heterostructures for optimal MOKE signals. The hBN encapsulation is particularly important since the wavelength and oxide thickness are usually more difficult to vary, while hBN flakes of various thicknesses can be easily found in a single exfoliation run. Therefore, in addition to protecting the 2DM against degradation, hBN encapsulation can be used as an active method for magneto-optical signal enhancement.

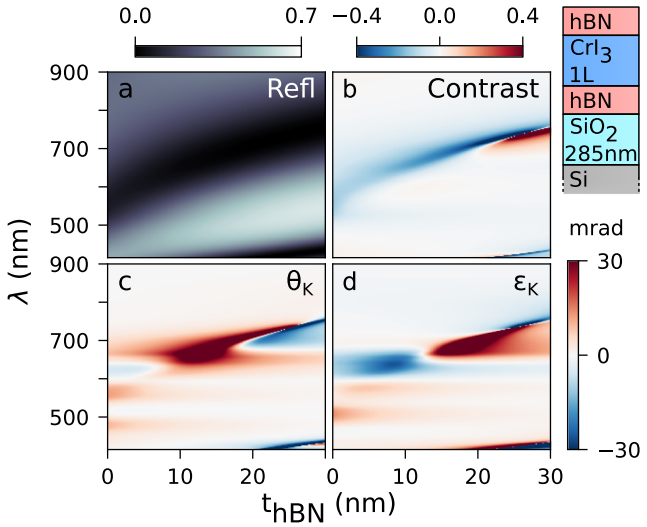

FIG. 4. Simulation results for a hBN-CrI_3(1L)-hBN-SiO_2(285 nm)-Si stack. (a) Reflectivity, (b) contrast, (c) Kerr rotation, and (d) ellipticity are shown as a function of wavelength and hBN thickness. Where the color scale is saturated, the values exceed the bounds of the scale.

That the common feature in the results of the simulation of the three systems above which θ_K and ε_K are maximized when the reflectivity is close to a minimum is a general and well-known phenomenon.[27,28,45] It can be explained by the behavior of the reflection coefficients for the electric field of the two circular polarizations, r_+ and r_-, near the reflectivity minimum. In this region, the magnitude of both reflection coefficients is small, and their complex phases change rapidly with wavelength and layer thickness. The exact parameter values around which these coefficients have a minimum and change phase are different for r_+ and r_- due to the circular birefringence and dichroism caused by the magnetic layer. Therefore, both the ellipticity, given by $\varepsilon_K = \tan^{-1}(|r_+| - |r_-|)/(|r_+| + |r_-|)$, and the Kerr rotation, given by $\theta_K = (\arg(r_+) - \arg(r_-))/2$, can become very large when the total reflectivity is near a minimum, as is explained in more detail in the supplementary material. On the other hand, if the reflectivity is large, both r_+ and r_- are large, meaning that their relative difference is small and that their complex phase changes slowly with wavelength and layer thickness. This will result in a low Kerr ellipticity and rotation, respectively. Therefore, the extreme MOKE signals of, e.g., $\varepsilon_K \approx \pm\pi/4$ and $\theta_K \approx \pi/2$ calculated for the CrI_3(bulk)-SiO_2(285 nm)-Si stack can only occur at a low reflectivity. This reasoning is not restricted to the samples treated in this paper. A general method to increase the Kerr rotation and ellipticity of a multi-layer sample is to use a combination of wavelength and thickness of the layers that minimizes the reflectivity. A reduction in the reflectivity, and a corresponding increase in the magneto-optical signals, can also be achieved by adding new layers to the sample. Such anti-reflection coatings have been used for over half a century to enhance Kerr signals from magnetic films.[27,29,46,47]

Here, we showed that thin-film interference can be a useful tool for improving magneto-optical signals in magnetic van der Waals systems. Through careful sample or heterostructure engineering, one is able to optimize their system for a particular experimental setup, improving the signal-to-noise ratio and measurement speed. The optimization of the signals can be carried out by choosing a particular illumination wavelength, substrate, thickness of the van der Waals magnet, or hBN used for encapsulation. The signal improvement, reaching several tens of milliradians, could lead to the identification of weaker signals from more delicate effects, such as chiral magnetic structures embedded in a homogeneously magnetized lattice.

See the supplementary material for the simulation details, graphs of the dielectric tensors used in the simulations, simulation results for other 2D magnetic monolayers, and an explanation for why the Kerr rotation and ellipticity are large when the reflectivity is close to a minimum.

We thank Alejandro Molina-Sánchez for sharing the data on the dielectric tensor for chromium trihalides. This work was supported by the Zernike Institute for Advanced Materials, the Dutch Research Council (NWO Start-Up, STU.019.014), and the European Union's Horizon 2020 Research and Innovation Programme under Grant Agreement No. 785219 (Graphene Flagship Core 3).

DATA AVAILABILITY

The data that support the findings of this study are available from the corresponding authors upon reasonable request.

REFERENCES

[1] D. Petit, A.-V. Jausovec, D. Read, and R. P. Cowburn, J. Appl. Phys. **103**, 114307 (2008).
[2] G. Rogez, B. Donnio, E. Terazzi, J.-L. Gallani, J.-P. Kappler, J.-P. Bucher, and M. Drillon, Adv. Mater. **21**, 4323 (2009).
[3] J. McCord, J. Phys. D: Appl. Phys. **48**, 333001 (2015).
[4] S. Jiang, L. Li, Z. Wang, K. F. Mak, and J. Shan, Nat. Nanotechnol. **13**, 549 (2018).
[5] M. Gibertini, M. Koperski, A. F. Morpurgo, and K. S. Novoselov, Nat. Nanotechnol. **14**, 408 (2019).
[6] W. Dickson, S. Takahashi, R. Pollard, R. Atkinson, and A. V. Zayats, IEEE Trans. Nanotechnol. **4**, 229 (2005).
[7] M. Savoini, F. Ciccacci, L. Duò, and M. Finazzi, Rev. Sci. Instrum. **82**, 023709 (2011).
[8] M. Lange, S. Guénon, F. Lever, R. Kleiner, and D. Koelle, Rev. Sci. Instrum. **88**, 123705 (2017).
[9] E. Beaurepaire, J.-C. Merle, A. Daunois, and J.-Y. Bigot, Phys. Rev. Lett. **76**, 4250 (1996).
[10] A. Kirilyuk, A. V. Kimel, and T. Rasing, Rev. Mod. Phys. **82**, 2731 (2010).
[11] B. Koopmans, G. Malinowski, F. Dalla Longa, D. Steiauf, M. Fähnle, T. Roth, M. Cinchetti, and M. Aeschlimann, Nat. Mater. **9**, 259 (2010).
[12] M. W. Wu, J. H. Jiang, and M. Q. Weng, Phys. Rep. **493**, 61 (2010).
[13] X.-X. Zhang, L. Li, D. Weber, J. Goldberger, K. F. Mak, and J. Shan, Nat. Mater. **19**, 838 (2020).
[14] B. Huang, G. Clark, E. Navarro-Moratalla, D. R. Klein, R. Cheng, K. L. Seyler, D. Zhong, E. Schmidgall, M. A. McGuire, D. H. Cobden, W. Yao, D. Xiao, P. Jarillo-Herrero, and X. Xu, Nature **546**, 270 (2017).
[15] C. Gong, L. Li, Z. Li, H. Ji, A. Stern, Y. Xia, T. Cao, W. Bao, C. Wang, Y. Wang, Z. Q. Qiu, R. J. Cava, S. G. Louie, J. Xia, and X. Zhang, Nature **546**, 265 (2017).
[16] M. Bonilla, S. Kolekar, Y. Ma, H. C. Diaz, V. Kalappattil, R. Das, T. Eggers, H. R. Gutierrez, M.-H. Phan, and M. Batzill, Nat. Nanotechnol. **13**, 289 (2018).
[17] Z. Fei, B. Huang, P. Malinowski, W. Wang, T. Song, J. Sanchez, W. Yao, D. Xiao, X. Zhu, A. F. May, W. Wu, D. H. Cobden, J.-H. Chu, and X. Xu, Nat. Mater. **17**, 778 (2018).
[18] K. S. Novoselov, A. K. Geim, S. V. Morozov, D. Jiang, Y. Zhang, S. V. Dubonos, I. V. Grigorieva, and A. A. Firsov, Science **306**, 666 (2004).
[19] D. S. L. Abergel, A. Russell, and V. I. Fal'ko, Appl. Phys. Lett. **91**, 063125 (2007).
[20] P. Blake, E. W. Hill, A. H. Castro Neto, K. S. Novoselov, D. Jiang, R. Yang, T. J. Booth, and A. K. Geim, Appl. Phys. Lett. **91**, 063124 (2007).
[21] A. Castellanos-Gomez, N. Agraït, and G. Rubio-Bollinger, Appl. Phys. Lett. **96**, 213116 (2010).
[22] D. J. Late, B. Liu, H. S. S. R. Matte, C. N. R. Rao, and V. P. Dravid, Adv. Funct. Mater. **22**, 1894 (2012).
[23] A. Castellanos-Gomez, E. Navarro-Moratalla, G. Mokry, J. Quereda, E. Pinilla-Cienfuegos, N. Agraït, H. S. J. van der Zant, E. Coronado, G. A. Steele, and G. Rubio-Bollinger, Nano Res. **6**, 191 (2013).
[24] H. Li, J. Wu, X. Huang, G. Lu, J. Yang, X. Lu, Q. Xiong, and H. Zhang, ACS Nano **7**, 10344 (2013).
[25] D. W. Berreman, J. Opt. Soc. Am. **62**, 502 (1972).
[26] P. Yeh, Surf. Sci. **96**, 41 (1980).
[27] M. Mansuripur, G. A. N. Connell, and J. W. Goodman, J. Appl. Phys. **53**, 4485 (1982).
[28] J. Zak, E. R. Moog, C. Liu, and S. D. Bader, J. Magn. Magn. Mater. **89**, 107 (1990).
[29] P. R. Cantwell, U. J. Gibson, D. A. Allwood, and H. A. M. MacLeod, J. Appl. Phys. **100**, 093910 (2006).
[30] S. Sumi, H. Awano, and M. Hayashi, Sci. Rep. **8**, 776 (2018).
[31] B. Bräuer, M. Fronk, D. Lehmann, D. R. Zahn, and G. Salvan, J. Phys. Chem. B **113**, 14957 (2009).
[32] J. Humlíček, in *Handbook of Ellipsometry*, edited by H. G. Tompkins and E. A. Irene (William Andrew Publishing, Norwich, NY, 2005), pp. 3–91.
[33] M. Schubert, in *Handbook of Ellipsometry*, edited by H. G. Tompkins and E. A. Irene (William Andrew Publishing, Norwich, NY, 2005), pp. 637–717.
[34] H. Fujiwara, *Spectroscopic Ellipsometry* (John Wiley & Sons, Ltd., 2007).
[35] B. Huang, G. Clark, D. R. Klein, D. MacNeill, E. Navarro-Moratalla, K. L. Seyler, N. Wilson, M. A. McGuire, D. H. Cobden, D. Xiao, W. Yao, P. Jarillo-Herrero, and X. Xu, Nat. Nanotechnol. **13**, 544 (2018).
[36] Z. Wang, T. Zhang, M. Ding, B. Dong, Y. Li, M. Chen, X. Li, J. Huang, H. Wang, X. Zhao, Y. Li, D. Li, C. Jia, L. Sun, H. Guo, Y. Ye, D. Sun, Y. Chen, T. Yang, J. Zhang, S. Ono, Z. Han, and Z. Zhang, Nat. Nanotechnol. **13**, 554 (2018).
[37] Y. Fang, S. Wu, Z.-Z. Zhu, and G.-Y. Guo, Phys. Rev. B **98**, 125416 (2018).
[38] Z. Ma, W. Zhu, G. Lin, Y. Liu, F. Jin, Y. Yang, T. Wu, X. Luo, Y. Sun, J. Chen, Y. Sun, C. Zhou, and Z. Sheng, AIP Adv. **9**, 125116 (2019).
[39] M. Wu, Z. Li, T. Cao, and S. G. Louie, Nat. Commun. **10**, 2371 (2019).
[40] C. Jin, Z. Tao, K. Kang, K. Watanabe, T. Taniguchi, K. F. Mak, and J. Shan, Nat. Mater. **19**, 1290 (2020).
[41] A. Molina-Sánchez, G. Catarina, D. Sangalli, and J. Fernández-Rossier, J. Mater. Chem. C **8**, 8856 (2020).
[42] C. M. Herzinger, B. Johs, W. A. McGahan, J. A. Woollam, and W. Paulson, J. Appl. Phys. **83**, 3323 (1998).
[43] P. M. Grant and G. B. Street, Bull. Am. Phys. Soc. **13**, 415 (1968).
[44] S.-Y. Lee, T.-Y. Jeong, S. Jung, and K.-J. Yee, Phys. Status Solidi B **256**, 1800417 (2019).
[45] M. Bass and V. N. Mahajan, *Handbook of Optics*, 3rd ed. (McGraw-Hill, 2009), Vol. I.
[46] J. Kranz and W. Drechsel, Z. Phys. **150**, 632 (1958).
[47] D. Kim, Y.-W. Oh, J. U. Kim, S. Lee, A. Baucour, J. Shin, K.-J. Kim, B.-G. Park, and M.-K. Seo, Nat. Commun. **11**, 5937 (2020).